Structural Basis for Homodimerization of the Src-associated during Mitosis, 68-kDa Protein (Sam68) Qua1 Domain*5*

Received for publication, March 23, 2010, and in revised form, May 19, 2010 Published, JBC Papers in Press, July 6, 2010, DOI 10.1074/jbc.M110.126185

N. Helge Meyer^{‡§}, Konstantinos Tripsianes^{‡§}, Michelle Vincendeau[¶], Tobias Madl^{‡§}, Fatiha Kateb^{‡§}, Ruth Brack-Werner¹, and Michael Sattler^{‡§1}

From the † Institute of Structural Biology, Helmholtz Zentrum München, Ingolstädter Landstrasse 1, 85764 Neuherberg, the [§]Munich Center for Integrated Protein Science (CiPS^M) at Department Chemie, Technische Universität München, Lichtenbergstrasse 4, 85747 Garching, and the ¶ Institute of Virology, Helmholtz Zentrum München, Ingolstädter Landstrasse 1, 85764 Neuherberg, Germany

Sam68 (Src-associated during mitosis, 68 kDa) is a prototypical member of the STAR (signal transducer and activator of RNA) family of RNA-binding proteins. STAR proteins bind mRNA targets and modulate cellular processes such as cell cycle regulation and tissue development in response to extracellular signals. Sam68 has been shown to modulate alternative splicing of the pre-mRNAs of CD44 and Bcl-xL, which are linked to tumor progression and apoptosis. Sam68 and other STAR proteins recognize bipartite RNA sequences and are thought to function as homodimers. However, the structural and functional roles of the self-association are not known. Here, we present the solution structure of the Sam68 Qua1 homodimerization domain. Each monomer consists of two antiparallel α -helices connected by a short loop. The two subunits are arranged perpendicular to each other in an unusual four-helix topology. Mutational analysis of Sam68 in vitro and in a cell-based assay revealed that the Qua1 domain and residues within the dimerization interface are essential for alternative splicing of a CD44 minigene. Together, our results indicate that the Qua1 homodimerization domain is required for regulation of alternative splicing by Sam68.

Sam68 ² (Src-associated during mitosis, 68 kDa) (1) belongs to the STAR (signal transducer and activator of RNA) family of RNAbinding proteins, which also includes Qk1 (quaking 1), SF1 (splicing factor 1), and Gld-1 (germline development defective-1) (2). STAR family proteins link signaling pathways and many aspects of RNA metabolism (splicing, localization, and translation). They are

regulated by post-translational modifications such as phosphorylation, acetylation, and arginine methylation (2).

Sam68 acts in post-transcriptional regulation of pre-mRNA splicing in response to extracellular signals (3). It is involved in a variety of pathways, including insulin and T-cell receptor signaling (4), and plays a key role in cell cycle regulation (5). Sam68 exhibits binding specificity for homopolymeric poly(U) RNA and has been shown to recognize UAAA or UUUA sequences with high affinity as determined by Systematic Evolution of Ligands by EXponential Enrichment (SELEX) and in vivo crosslinking (6, 7). Post-translational modifications can regulate Sam68 function by critically affecting the accessibility to RNA (8, 9). Tyrosine phosphorylation by Src kinase during mitosis enhances the interaction of Sam68 with Ras-GAP (10) but prevents its association with RNA. On the other hand, acetylation of lysine residues by histone acetyltransferases enhances RNA binding (11). Finally, overexpression of Sam68 has been linked to prostate cancer, cell proliferation, and survival (12).

Sam68 has been identified as a key determinant in the alternative splicing of various important RNA targets, like CD44 (13) and Bcl-x_L (14), which are linked to apoptosis and cancer. In particular, alternative splicing of CD44 impacts embryonic development and immune response (15-18). Up to 10 variant exon sequences can be included in the mature CD44 mRNA. Among them, variable exon 5 (exon v5) inclusion is associated with tumor progression and T-cell activation (17, 19). Sam68 is a target for phosphorylation by extracellular-signal-regulated kinase (ERK), which promotes inclusion of CD44 exon v5 in response to Ras activation by phorbol ester stimulation. Sam68 binds two RNA sequences within exon v5 and the preceding intron, respectively (9, 13). Recent studies indicate that Sam68 interacts with the heterodimeric splicing factor U2AF (U2 small nuclear ribonucleoprotein particle auxiliary factor) (9). Recognition of the 3' splice site by U2AF is a key step in spliceosome formation. The interaction with Sam68 is thought to stabilize U2AF binding to its cognate RNA elements. Interestingly, phosphorylation of Sam68 by ERK interferes with RNA binding and reduces pre-mRNA occupancy by U2AF. Altogether, these data indicate that Sam68 can regulate alternative splicing in a signal-dependent manner.

Sam68 shares high similarity with SF1, another binding partner of U2AF. The so-called STAR domain, also referred to as GRP33/SAM68/GLD1 domain, consists of an hnRNP K homology (KH) domain flanked by two domains N- and C-terminal of



^{*} This work was supported by a grant from the Deutsche Forschungsgemeinschaft and grants from the Alexander von Humboldt foundation (to K.T. and F. K.) and an EMBO fellowship (to T. M.).

[♦] This article was selected as a Paper of the Week.

The atomic coordinates and structure factors (code 2XA6) have been deposited in the Protein Data Bank, Research Collaboratory for Structural Bioinformatics, Rutgers University, New Brunswick, NJ (http://www.rcsb.org/).

The chemical shifts can be accessed through the Biological Magnetic Resonance Bank (BMRB) under BMRB accession number 16969.

The on-line version of this article (available at http://www.jbc.org) contains supplemental Figs. 1–7.

¹ To whom correspondence should be addressed. Tel.: 49-89-289-13418; Fax: 49-89-289-13869; E-mail: sattler@helmholtz-muenchen.de.

² The abbreviations used are: Sam68, Src-associated during mitosis, 68-kDa protein; STAR, signal transducer and activator of RNA; SF1, splicing factor 1; Gld-1, germline development defective-1; U2AF, U2 small nuclear ribonucleoprotein particle auxiliary factor; KH, hnRNP K homology; HSQC, heteronuclear single-quantum correlation; r.m.s.d., root mean square deviation.

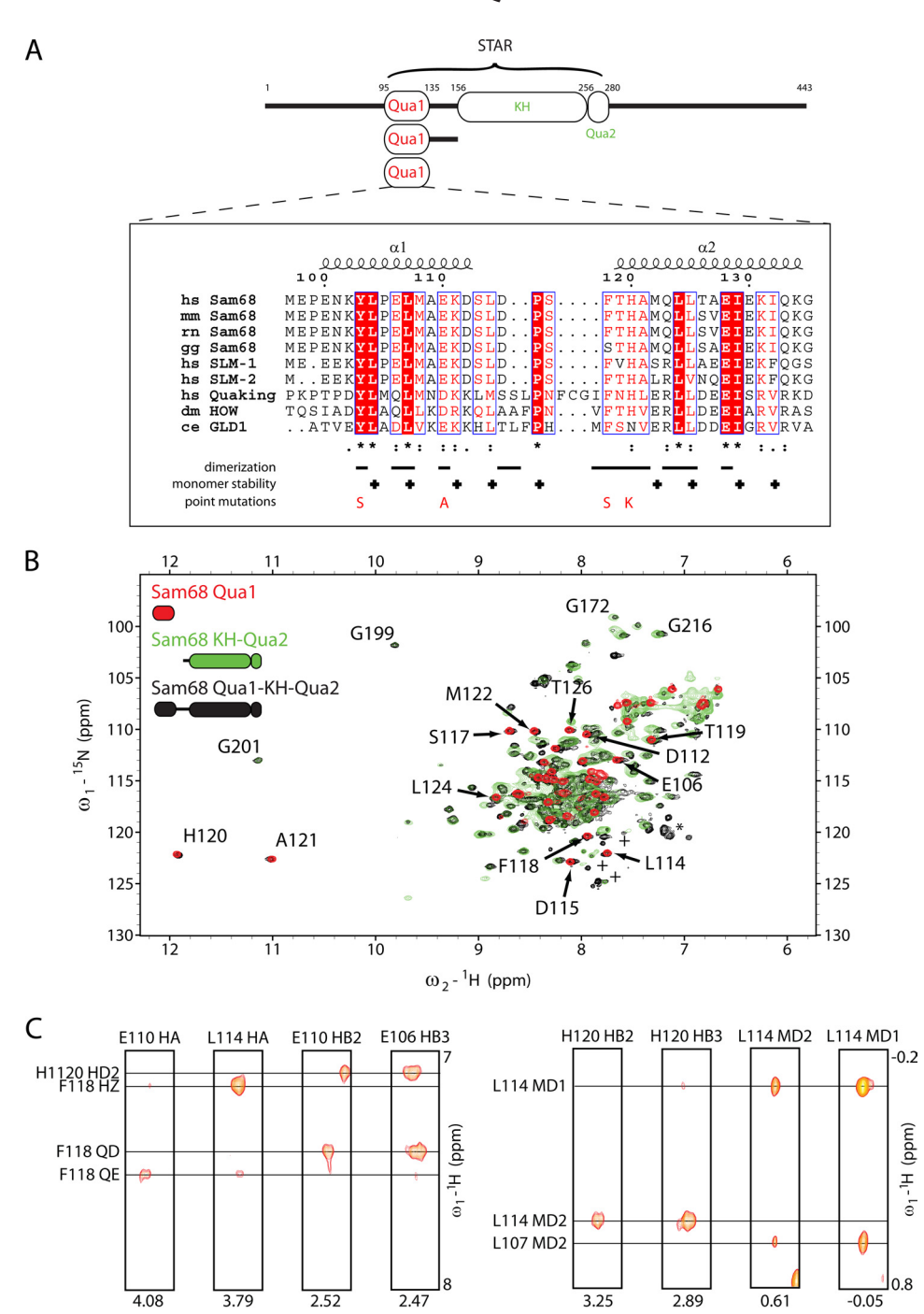


FIGURE 1. **Topology and NMR spectra of the Sam68 STAR domain.** *A*, domain organization of Sam68. The Qua1 proteins used for NMR are indicated. The sequence alignment of the Qua1 domains of different members in the STAR family is shown, and residue numbers are given for Sam68 Qua1. The secondary structure of Sam68 Qua1 is depicted above the alignment. Residues important for monomer and dimer stability are indicated below, by — and +, respectively. Conserved residues that were mutated are indicated. Sequences were aligned using the program ClustalW (51) and analyzed using the program ESpript (52). Abbreviations used are: *hs, H. sapiens*; mm, *Mus musculus*; *rn, Rattus norvegicus*; *gg, Gallus gallus domesticus*; *dm, Drosophila melanogaster*; *ce, Caenorhabditis elegans. B*, overlay of a ¹H, ¹⁵N TROSY spectrum of perdeuterated Qua1-KH-Qua2 (residues 95–280) (*blue*) and ¹H, ¹⁵N HSQC spectra of Qua1 (residues 95–135) (*red*) and KH-Qua2 (residues 147–280) (*green*). Note that the linker connecting the Qua1 and KH domains (135–156) is not included in the Qua1 protein. Signals arising from arginine side chains are marked with an *asterisk*, and some small peaks of degradation products are marked with +. *C*, intermolecular NOEs recorded on an asymmetrically ¹⁵N/¹³C-labeled sample.

the KH domain, referred to as Qua1 and Qua2, respectively (2, 3). Interestingly, SF1 is the only known member devoid of the Qua1 subdomain and functions as a monomer (20). The KH

 ω_2 -1H (ppm)

domain is one of the major RNA binding motifs in eukaryotic cells (21). The structural basis for the recognition of single-stranded RNA by the KH-Qua2 domain of SF1 has been described, indicating that the Qua2 domain extends the KH fold and that the KH-Qua2 tandem domain is essential for sequencespecific RNA recognition (22). The solution structure of the free form of the KH-Qua2 region of Quaking showed that the Qua2 helix does not contact the KH domain in the absence of RNA (23). Biochemical data and in vivo studies suggest that the Qua1 domain can oligomerize (24-27). However, the structural basis for oligomerization and the role for the in vivo function of STAR proteins are unknown.

Here, we present the NMR solution structure of the Sam68 Qua1 domain. Qua1 forms a homodimer composed of a perpendicular interaction of two helical hairpins. A network of hydrophobic and electrostatic interactions stabilizes the dimer interface. Based on NMR and biophysical data, we show that the Qua1 domain is sufficient for homodimerization of Sam68 in vitro. Cell-based splicing assays identify critical residues in the dimer interface and reveal that Qua1 is necessary for the function of Sam68 in alternative splicing.

EXPERIMENTAL PROCEDURES

Sample Preparation—Homo sapiens Sam68 Qua1(95-135), Qua1(95-156), KH-Qua2(147-280), and Qua1-KH-Qua2(95-280), which were derived from pcDNA 3.1 HsSam68 described in Ref. 13, were cloned in a modified pETM-11 vector (European Molecular Biology Laboratory) containing an additional N-terminal double Z-tag and expressed in Escherichia coli BL21(DE3). Point mutations were introduced in pcDNA 3.1 HsSam68 and pETM-11 ZZ Qua1(95-135) using the QuikChange site-directed mutagenesis (Invitrogen) protocol. The

corresponding proteins contain two additional residues at the N-terminal tobacco etch virus protease cleavage site, which are derived from the expression vector.



 ω_2 -1H (ppm)

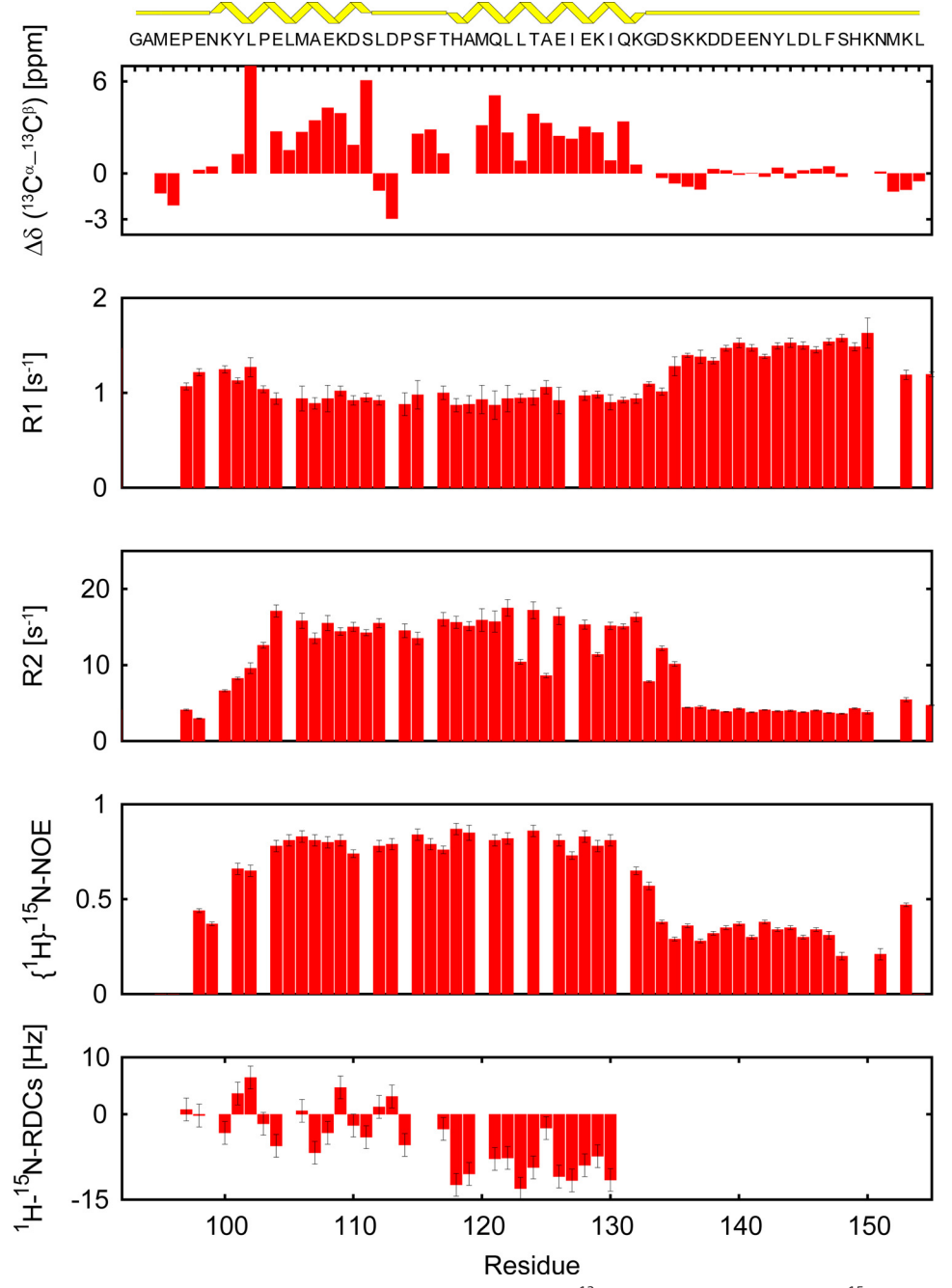


FIGURE 2. NMR characterization of the Sam68 Qual domain. ¹³C secondary chemical shifts, ¹⁵N R1, R2 relaxation rates, {1H}-15N heteronuclear NOE, and 1H-15N residual dipolar couplings (RDCs) are plotted versus Sam68 Qua1 residue numbers. The secondary structure is indicated at the *top. Error bars* for ¹⁵N relaxation data are estimated from the noise level as described in Ref. 33. Error bars for RDCs are estimated based on spectral

Bacteria were grown in LB medium for preparation of unlabeled sample or M9 medium supplemented with ¹³C-labeled glucose and/or [15N]H₄Cl for uniformly labeled samples, respectively. The protein was expressed at 20 °C for 16 h after induction with 250 mм IPTG.

Proteins were purified using Ni²⁺ affinity chromatography (nickel-nitrilotriacetic acid, Qiagen). After cleavage of the His and the Z-tag with tobacco etch virus protease, the tags were separated from the protein by a second Ni²⁺ affinity step. Qua1 samples were heat-shocked for 5 min at 85 °C. The samples were further purified by size exclusion chromatography on a HiLoad 16/60 Superdex 75

(GE Healthcare) and kept in 10 mm phosphate, pH 6.5, 100 mm NaCl.

An asymmetrically labeled sample to record intermolecular NOEs was prepared as follows. Equimolar amounts of unlabeled and 15N/ ¹³C uniformly labeled Qua1 (residues 95-135) were mixed and incubated with 1% SDS at 85 °C for 10 min. After slowly cooling down, SDS was removed by dilution and ultra filtration using a 15-ml Amicon (Millipore) with a molecular weight cutoff of 5,000.

NMR Spectroscopy—NMR measurements were carried out at 298 K on a Bruker Avance III 750-MHz spectrometer equipped with a TXI probe head, a 600-MHz spectrometer equipped with a TCI cryo-probe head or on an Avance 900 instrument equipped with a TXI cryoprobe head. Spectra were processed with NMRPipe (28) and analyzed with Sparky (29). Backbone assignment was done semiautomatically using MARS (30). For backbone and side chain assignment CBCA(CO)NH, CBCANH (H)CCH-TOCSY spectra were recorded (31). Distance information was obtained from 15N- and 13C-edited NOESY spectra with a mixing time of 70 ms. To distinguish interand intramolecular NOEs, a set of isotope-edited and filtered NOESY spectra was recorded (31, 32). Experiments were carried out using a 1 mm uniformly ¹⁵N/¹³C-labeled or 2 mm asymmetrically $^{15}\mathrm{N}/^{13}\mathrm{C}$ labeled Qua1(95-156) sample, respectively. 15N R₁ and R₂ relaxations rates and {1H}-15N heteronuclear NOE data were measured at a 750-MHz proton Larmor frequency and 298 K as described (33). H^{α} - C^{α} , N-C' and HN-N residual dipolar couplings

were recorded using HNCO-based NMR experiments (34) with a 1 mm Qua1(95-135) sample that was aligned in a medium containing 15 mg/ml Pf1 phage (Profos AG, Regensburg, Germany) as described (35). Paramagnetic relaxation enhancements were measured from saturation recovery ¹H, ¹⁵N HSQC experiments (recovery times between 0.01 and 4.0 s) at concentrations of 0, 1, 2, 3, 4, 5, 7, and 10 mm of the soluble paramagnetic agent gadolinium diethylenetriaminepentaacetic acid bismethylamide (Gd(DTPA-BMA)). Back-calculation and data analysis were carried out according to Ref. 36.

Structure Calculation—Automated NOE cross-peak assignment was performed using the software CYANA 3.0 (37). Automatically assigned NOEs and completeness of the NOE cross-peaks were manually inspected. Homodimer symmetry is explicitly taken into account for network anchoring, and identical conformation of the two monomers is ensured by dihedral angle difference restraints for all corresponding torsion angles. Additionally, a symmetric relative orientation of the two monomers is maintained by distance difference restraints between symmetry-related intermolecular C^{α} - C^{α} distances (38). Distance restraints from the CYANA calculationand TALOS+ (39)-derived torsion angles and the residual dipolar coupling restraints were used in a water refinement calculation (40) with Aria 2.2 (41). The quality of the structure ensemble was validated using the iCING³ web server as well as PROCHECK (43) and WHATCHECK (44). Molecular images were generated using PyMOL (45).

Circular Dichroism (CD) Spectroscopy—Temperature series of far-UV (190–250 nm) CD spectra were recorded on 100 μ M Qua1 wild type or mutant proteins in 20 mM phosphate, pH 6.5, 50 mM NaCl using a JASCO J-715 spectropolarimeter.

Cell Culture and Transfections—U138MG cells were cultured as described previously (46). All overexpression experiments were performed in 6-well plates. Cells were seeded at a density of 2 \times 10⁵ cells/well 1 day prior to transfection and cultured for 30 h after transfection. Transfections were performed using FuGENE® HD transfection reagent (Roche Diagnostics) according to the manufacturer's instructions. For cotransfection experiments, 2 μ g of CD44 v5 minigene-plasmid DNA (13) was co-transfected with 300 ng of plasmids expressing Sam68 or wild type or mutants. As a control, the CD44 v5 minigene-plasmid DNA was co-transfected with 300 ng of the pcDNA 3.1 expression plasmid. Expression of all proteins was checked by Western blot analysis (data not shown).

 $\it RT-PCR$ $\it Analysis$ —Cytoplasmic RNA was prepared using the PARIS kit (Ambion) according to the manufacturer's protocol. 1 units/ μg of RNA was transcribed with SuperScript II (Invitrogen) according to the manufacturer's protocol, using random hexamers. RT-PCR analyses were carried out as described in Ref. 13 using 25 PCR cycles. RT-PCR bands were quantified densitometrically using the ImageJ Software. Three independent experiments were performed.

RESULTS

Qua1 Is Sufficient for Sam68 Homodimerization—It has been shown that the STAR domain of Sam68 (Fig. 1A) and other members of the STAR family dimerize (24–27). The apparent molecular mass estimated from size exclusion chromatography of \sim 40 kDa is consistent with a dimer of the Sam68 STAR domain (not shown). To identify the region that mediates dimerization, we expressed proteins comprising the Qua1, KH-Qua2, and Qua1-KH-Qua2 domains in *E. coli*. An overlay of 1 H, 15 N correlation NMR spectra of the Qua1 (residues 95–135) and KH-Qua2 (residues 147–280) subdomains with that of the STAR domain (residues 95–280) shows that chemical shifts

TABLE 1

Structural statistics of the Sam68 Qua1 homodimer

NOE-based distance restraints^a

Medium range $(2 \le |i - j| \le 4)$

Intraresidual, sequential

Disallowed regions

Statistics are given for the 20 lowest energy structures after water refinement out of 100 calculated. The CNS $E_{\rm repel}$ function was used to simulate van der Waals interactions with an energy constant of 25 kcal mol $^{-1}$ Å $^{-4}$ using PROLSQ van der Waals radii (40). r.m.s.d. and PROCHECK values apply for residues 101–135.

950

504

| Long range ($ i - j \ge 5$) | 316 |
|---|---|
| Intermolecular | 456 |
| Total | 2226 |
| Other restraints | |
| $\phi + \psi$ dihedral angle restraints | 128 |
| Residual dipolar coupling restraints $(H^N-N, N-C', H^{\alpha}-C^{\alpha})$ | 128 |
| Coordinate precision r.m.s.d. | |
| Backbone (Å) | 0.32 ± 0.09 |
| Heavy atom (Å) | 0.97 ± 0.16 |
| Consistency (structure vs. restraints) | |
| r.m.s.d. (Å) from experimental distance restraints ^a | 0.019 ± 0.002 |
| r.m.s.d. (°) from experimental torsion angle | 0.911 ± 0.104 |
| restraints ^b | |
| restraints ^b RDC Q-factor ^c | 0.230 ± 0.005 |
| | 0.230 ± 0.005 Structure Z-score |
| | |
| RDC Q-factor ^c | |
| RDC Q-factor ^c WHATCHECK ^d | Structure Z-score |
| RDC Q-factor ^c WHATCHECK ^d First generation packing quality | Structure Z-score 0.497 |
| RDC Q-factor ^c WHATCHECK ^d First generation packing quality Second generation packing quality | 0.497 -0.028 |
| RDC Q-factor ^c WHATCHECK ^d First generation packing quality Second generation packing quality Ramachandran plot appearance | 0.497 -0.028 0.010 |
| RDC Q-factor ^c WHATCHECK ^d First generation packing quality Second generation packing quality Ramachandran plot appearance χ_1/χ_2 rotamer normality | 0.497 -0.028 0.010 -2.057 |
| RDC Q-factor ^c WHATCHECK ^d First generation packing quality Second generation packing quality Ramachandran plot appearance χ_1/χ_2 rotamer normality Backbone conformation | 0.497 -0.028 0.010 -2.057 |
| RDC Q-factor ^c WHATCHECK ^d First generation packing quality Second generation packing quality Ramachandran plot appearance χ_1/χ_2 rotamer normality Backbone conformation Ramchandran plot ^d | 0.497 -0.028 0.010 -2.057 1.325 |

 $[^]a$ Distance restraints were employed with a soft square well potential using an energy constant of 50 kcal mol $^{-1}$ Å $^{-2}$. No distance restraint was violated by more than 0.5 Å. b Torsion angle restraints derived from TALOS (39) were applied to φ , ψ backbone

seen in the smaller domains are very similar to those of common residues in the STAR domain. This indicates that there are no strong contacts between Qua1 and KH-Qua2 and that these two regions are structurally autonomous (Fig. 1*B*).

The ¹H NMR frequencies in the ¹H, ¹⁵N HSQC spectrum of Qua1 (residues 95-156) are mainly found within a small region centered around 8 ppm, indicating the presence of mostly helical and random coil conformation. Analysis of the 13 C $^{\alpha/\beta}$ secondary chemical shifts reveals that residues 95–135 comprise two α -helices that are interconnected by a short loop. The 20 C-terminal amino acids (residues 136 – 156) do not exhibit any secondary structure. ¹⁵N R₁ and R₂ relaxation rates as well as {¹H}-¹⁵N heteronuclear NOE data show that the C terminus is highly flexible, whereas the loop connecting the two helices has a slightly increased flexibility when compared with the helical segments (Fig. 2). Thus, only residues 95-135 define the globular fold of the Qua1 domain. A tumbling correlation time of $\tau_c = 9.5$ ns was estimated from the $^{15}{\rm N}~{\rm R}_2/{\rm R}_1$ relaxation rates ratio for Qua1, consistent with the molecular mass expected for a homodimer (14 kDa). Even at concentrations of 10 μM, there is no significant change in the 15 N relaxation rates and thus τ_c (data not shown), indicating that the dimerization constant is at least in the low micromolar to nanomolar range. Additionally,



³ G. W. Vuister, J. F. Doreleijers, and A. W. Sousa da Silva, manuscript in preparation.

angles using energy constants of 200 kcal mol⁻¹ radians⁻². No dihedral angle restraint was violated by more than 5°.

 $[^]c$ Residual dipolar couplings (RDCs) were employed with a harmonic potential using an energy constant of 0.5 kcal mol $^{-1}$ Hz $^{-2}$ Q-factor as defined in Ref. 42.

^d PROCHECK (43) and WHATCHECK (44) were used to determine the quality of the structure. Positive WHATCHECK Z-scores indicate that structure is better than average.

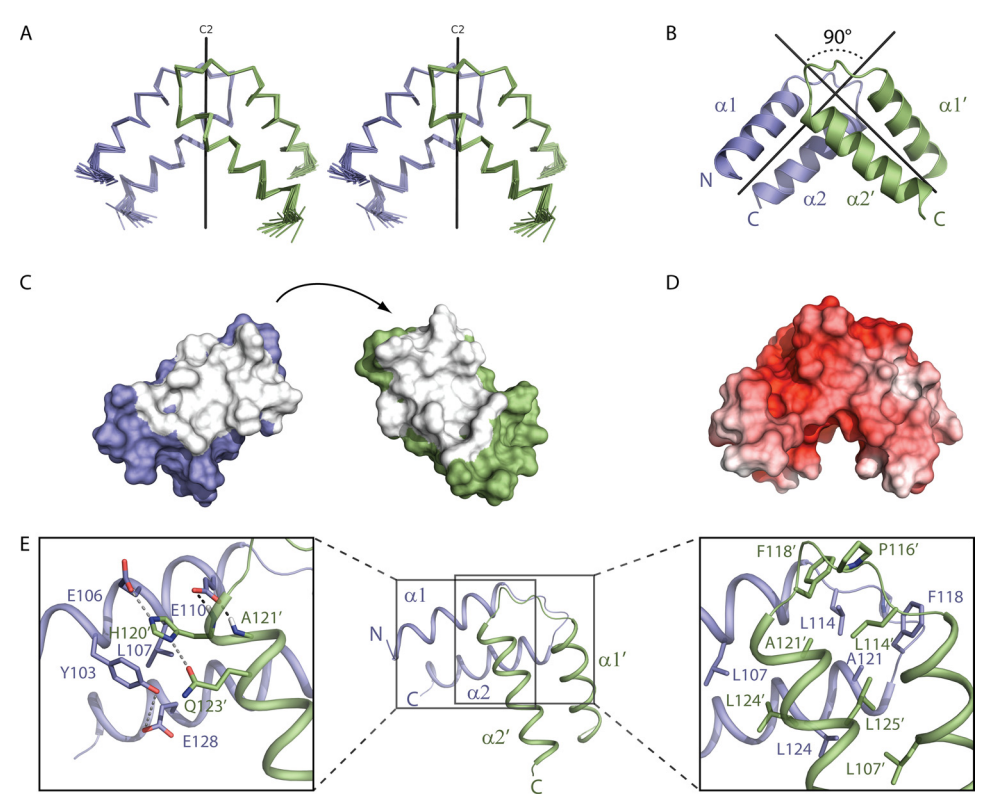


FIGURE 3. NMR structure of the Sam68 Qua1 homodimer. A, stereo view of the ensemble of the 20 lowest energy structures. B, ribbon representation of the Sam68 Qua1 dimerization domain. C, surface representation of two separated Qua1 monomers, showing a view onto the dimer interface (white). D, surface representation colored according to electrostatic surface potential at $\pm 7~k_B$ T/e (temperature/electron charge) for positive (blue) or negative (red) charge potential using the program APBS (53). E, close-up view of the interface. Side chains of key residues in the dimer interface are shown as sticks. Hydrogen bonds between the Glu-110 side chain and the His-120 and Ala-121 amides are indicated by black dashed lines. Potential hydrogen bonds and electrostatic interactions are shown by gray dashed lines.

the apparent molecular weight determined by size exclusion chromatography matches well with a homodimer (supplemental Fig. 1). These observations suggest that the Qua1 domain is sufficient for homodimerization.

For structural analysis and to further confirm that Qua1 is a homodimer, we attempted to identify intermolecular NOEs. In the case of a symmetric homodimer, the NOESY spectrum contains both intramolecular and intermolecular cross-peaks. To unambiguously distinguish intermolecular from intramolecular NOEs, isotope-filtered experiments were recorded on an asymmetrically ¹⁵N/¹³C-labeled sample (31, 32). To obtain such a sample, equimolar amounts of uniformly ¹⁵N/¹³C-labeled and unlabeled Qua1 are mixed. Random exchange of the subunits yields 50% of asymmetrically isotope-labeled dimers. Isotope-edited/filtered NMR experiments will detect exclusively intermolecular NOEs for this population, whereas no signals are observed for symmetrically labeled or unlabeled homodimers or monomeric species. Thermal denaturation in presence of 1% SDS and refolding of equal amounts of labeled and unlabeled Qua1 resulted in a fingerprint spectrum identical to that of the native protein, indicating that the fold was restored (data not shown). After refolding, more than 100 intermolecular cross-peaks were observed in an isotope-edited/filtered NOESY experiment (Fig. 1C). Taken together, these data establish that Qua1 is a stable homodimer.

Structure of the Sam68 Qua1 Homodimer-We determined the solution structure of the Sam68 Qua1 homodimer (comprising residues 95-135) by heteronuclear triple-resonance NMR spectroscopy using uniformly as well as asymmetrically labeled 15N/13C-labeled protein. The structure is defined based on 2226 experimental distance restraints, including 2×228 intermolecular distance restraints, derived from 13C- and 15N-edited NOESY HSQC spectra as well as ¹³C/¹⁵N-filtered, ¹⁵N- or ¹³C-edited NOESY-HSQC spectra. A summary of the structural and restraint statistics is given in Table 1. The ensemble of the 20 lowest energy structures obtained after water refinement is shown in Fig. 3A. The quality of the structures was further validated by comparison of measured and back-calculated relaxation rate enhancements upon the addition of the paramagnetic co-solvent Gd(DTPA-BMA) (36), which showed excellent agreement (supplemental Fig. 2).

Each Qua1 monomer comprises two α -helices that are aligned in an antiparallel fashion with a tilt angle

of \sim 30°, connected by a short loop. Hydrophobic residues are spaced every 3-4 residues apart on each helix and interact with residues arrayed on the other helix of the same monomer, i.e. Leu-104, Leu-107, Lys-111 and Leu-114 in helix α 1 contact Ile-132, Ile-129, Leu-125, and Met-122 in helix α 2, respectively (supplemental Fig. 3). This arrangement is reminiscent of a short "zipper" where the extensive hydrophobic contacts lead to a tight packing of the two helices of each monomer. A potential side-chain hydrogen bond between the invariant Tyr-103 (helix α 1) and Glu-128 (helix α 2) further stabilizes the helical hairpin. The lack of the corresponding hydrogen bond may be consistent with a lethal phenotype of the E48G mutation in the mouse Qk1 paralog (Glu-48 corresponds to Sam68 Glu-128). Another important feature of this topology is the highly conserved Pro-116 in the loop connecting the two helices, which allows the reversal of the peptide backbone.

The Qua1 dimer is formed by perpendicular stacking of the two monomers with a C2 symmetry (Fig. 3, A and B). Numerous hydrophobic contacts, which mainly involve the loop region connecting the two helices, stabilize the dimer interface. Below this largely hydrophobic contact area, cross-subunit hydrogen bonds and electrostatic contacts between the N-terminal end of helix $\alpha 2$ and the $\alpha 1'/\alpha 2'$ helices of the other monomer provide additional intersubunit interactions (Fig. 3). The interface area covers 624



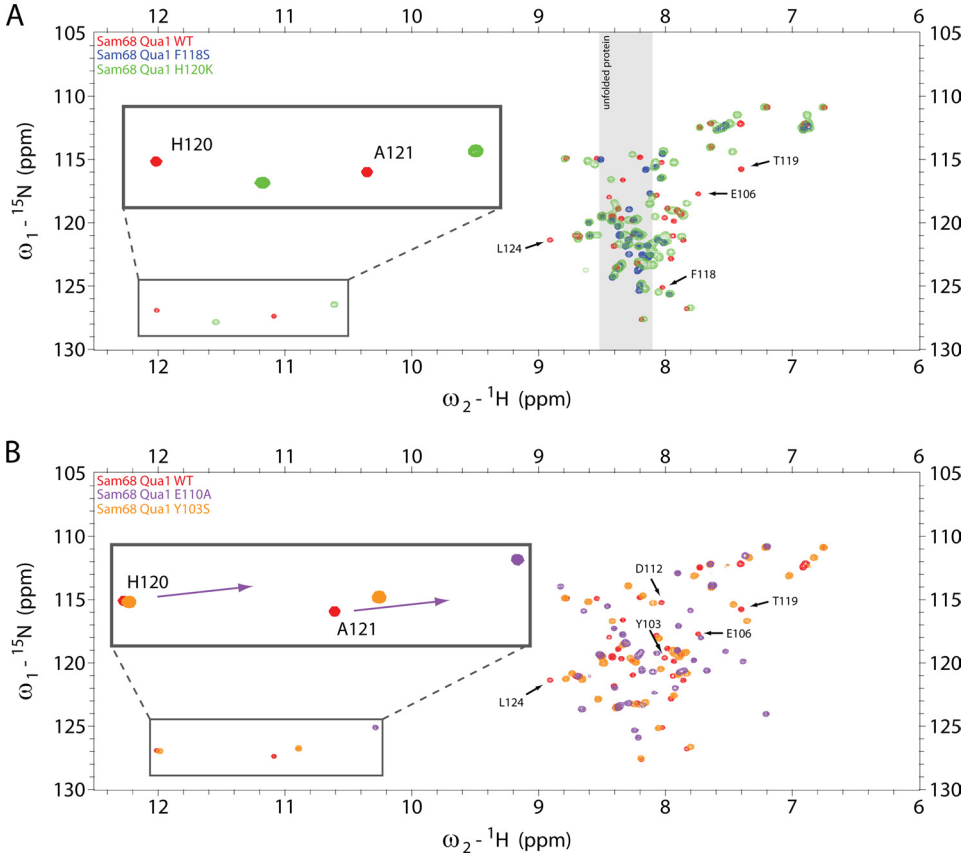


FIGURE 4. NMR spectra of wild type and mutant Sam68 Qua1. A and B, overlay of the ¹H, ¹⁵N HSQC spectra of the different Qua1 mutants that disrupt the overall fold (A) or that have mainly local structural effects (B). A, the F118S mutant is unfolded as shown by a drastically reduced chemical shift dispersion. The typical chemical shift range for unfolded proteins is indicated by a gray box. The H120K mutant shows two sets of NMR signals, which account for folded and unfolded moieties of the protein (see supplemental Fig. 4). B, the mutants Y103S and E110A are folded. However, the intermolecular hydrogen bond between the Glu-110 side chain and the backbone amides of His-120 and Ala-121 cannot form in the E110A mutant, resulting in an upfield shift of the backbone amide resonances for those residues (indicated by arrows). The E110A mutant may lead to a local rearrangement of the aromatic side chains of His-120 and indirectly of Tyr-103, which is reflected by the overall chemical shift differences when compared with the wild type protein. Similarly, the relatively large changes of the NMR chemical shifts in the Y103S mutant may be attributed to the removal of aromatic ring current effects.

 $Å^2$ /monomer, which accounts for more than 18% of the total surface area of one monomer (Fig. 3*C*).

A key determinant of the dimer formation is the almost invariant Phe-118 in the α 1- α 2 loop. Its aromatic side chain stacks with the Leu-114' side chain from the other monomer (Fig. 3E, right). The side chains of Leu-107, Ala-121, Leu-124, and Leu-125 mediate additional hydrophobic interactions stabilizing the dimer interface. Near the intersection of the $\alpha 2/\alpha 2'$ helices, the His-120' side chain contacts the aromatic ring of Tyr-103 in the other monomer. Apart from this hydrophobic network, cross-subunit hydrogen bonds between Glu-110 and the backbone amide protons of Ala-121' and His-120' are observed (Fig. 3E, left). This is reflected by large downfield shifts of the ¹H NMR frequencies of the backbone amides of Ala-121 and His-120 (Fig. 4). Furthermore, the side chain of His-120' is in close proximity to the side chains of Glu-106 and Gln-123', implying electrostatic stabilization (Fig. 3E, left). Charged residues are distributed at the periphery and at the opposite side of the interface, giving an overall negative charge to the Qua1 homodimer (Fig. 3D).

An arrangement of two antiparallel helices is a common feature in a variety of different proteins and protein folds. However, structural similarity searches (47) did not reveal any structure in the Protein Data Bank (PDB) database with a similar perpendicular arrangement of two helical hairpins, indicating that the Qua1 homodimer adopts a novel four-helix dimer topology.

Mutational Analysis of the Dimer Interface—We confirmed the dimer contacts seen in the structure by mutational analysis. Various single point mutations were designed, and ¹H, ¹⁵N HSQC experiments of the corresponding proteins were recorded to monitor the influence of the mutation on the overall fold. The capability to form homodimers was determined by analysis of apparent local correlation times, $\tau_c^{\rm app}$, estimated from the ¹⁵N relaxation data. The $au_c^{
m app}$ values reflect the size of the protein tumbling in solution, and the distribution of τ_c^{app} therefore allows estimating the ratio between the monomeric and the dimeric forms (supplemental Fig. 4).

Mutation of Phe-118 (F118S) leads to a virtually complete loss of structure and dimerization (Fig. 4A). Remarkably, at concentrations above 1 mm, a small portion of the protein can still dimerize, as indicated by weak NMR signals in the

¹H, ¹⁵N HSOC, which reflect the folded dimer (data not shown). The H120K variant is in slow exchange between unfolded protein and structurally intact dimer, as indicated by two sets of signals with distinct ¹⁵N relaxation properties that are observed in the ¹H, ¹⁵N HSQC spectra (Fig. 4A). The Y103S and E110A variants maintain the overall fold, and the protein still forms dimers (Fig. 4B). However the distribution of local correlation times, τ_c^{app} , derived from the NMR relaxation data (supplemental Fig. 4) is slightly decreased in both mutants when compared with the wild type, consistent with a fast exchange between monomeric and dimeric species. The effect of the E110A mutation on dimerization is more pronounced as the average τ_c^{app} measured for the E110A variant is lower than for the Y103S mutant. The E110A Qua1 domain cannot form intermolecular hydrogen bonds to the backbone amides of Ala-121' and His-120'. This results in an upfield shift of the respective resonances seen in the ¹H, ¹⁵N HSQC spectrum of the E110A mutant (Fig. 4B). Thermal denaturation of the Qua1 mutants followed by CD spectroscopy demonstrates that the thermal stability of the Y103S and E110A variants is decreased when compared with



the wild type protein (supplemental Fig. 5), although both mutants are still mainly dimeric. In contrast, the F118S and H120K mutants are highly unstable or already unfolded at room temperature (data not shown).

In summary, the structure-guided mutagenesis shows a good correlation between the importance of contacts in the interface and dimer formation. Specifically, the F118S mutation completely disrupts the dimer, whereas the other mutations appear to have more local effects only destabilizing the Qua1 dimer.

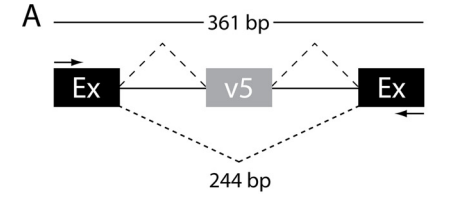
Functional Qua1 Domain Is Required for Splicing Regulation by Sam68—Sam68 has previously been shown to increase the inclusion of the CD44 exon v5 in mRNAs produced from a CD44v5 minigene (Fig. 5A) (13). Here, we used this assay to investigate whether the Qua1 domain is required for regulation of splicing by Sam68. These experiments were performed in the human astrocytic cell line U138MG because human astrocytes were previously reported to express relatively low levels of endogenous Sam68 (48) (supplemental Fig. 6). Overexpression of wild type full-length Sam68 led to a more than 3-fold increase of exon v5 inclusion (Fig. 5, B and C). As expected, a mutant lacking the KH region, which mediates RNA binding, failed to increase exon v5 inclusion. Interestingly, the mutant lacking the Qua1 domain was similarly ineffective as the Δ KH mutant in this assay. This demonstrates that the Qua1 domain is essential for Sam68 activity in vivo. The same effect is observed for the F118S variant, which in vitro, in the context of the Qua1 domain, does not dimerize. H120K, which is disturbed in dimerization in vitro (supplemental Fig. 4), has significantly reduced splicing activity. In contrast, the E110A mutant is only slightly destabilized in vitro, and, consistently, supports alternative splicing almost as the wild type protein. Although mutation of Tyr-103 has the least effect on dimerization in vitro, it seems to be crucial for Sam68 activity as the Y103S variant is virtually inactive in the splicing assay.

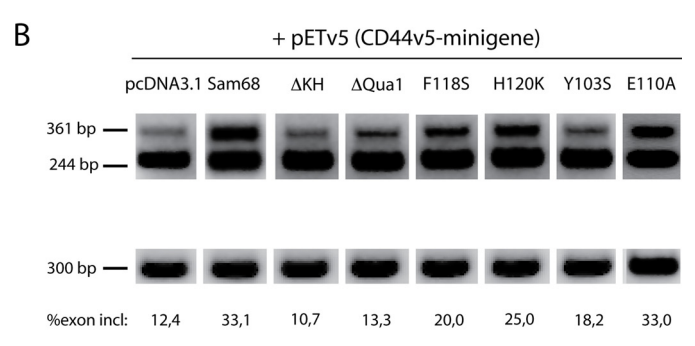
DISCUSSION

We show that the Sam68 Qual domain adopts a unique four-helix dimer fold with the two monomers stacking perpendicularly. The dimer interface is stabilized by a combination of hydrophobic interactions and cross-subunit hydrogen bonds. Residues that mediate these interactions are highly conserved (Fig. 1A). We demonstrated that mutations of critical residues that build the dimer interface impair the quaternary arrangement. The Qual domain is highly conserved within the STAR family, with the exception of the loop region, implying that the Qua1 dimeric structures of these proteins are similar.

In fact, while this manuscript was in preparation, the crystal structure of the Gld-1 Qua1 dimer (PDB 3K6T) was reported (49) with the same topology described here for Sam68. The two structures superimpose very well (backbone coordinate r.m.s.d. 1.1 Å; supplemental Fig. 7), although local differences are seen for intermolecular contacts in the loop region, presumably linked to its different composition.

Our results demonstrate that the Qua1 domain alone is sufficient for dimerization of the Sam68 STAR domain. Although we cannot strictly exclude additional contributions from the KH-Qua2 domain to the dimer interface (25), it seems likely





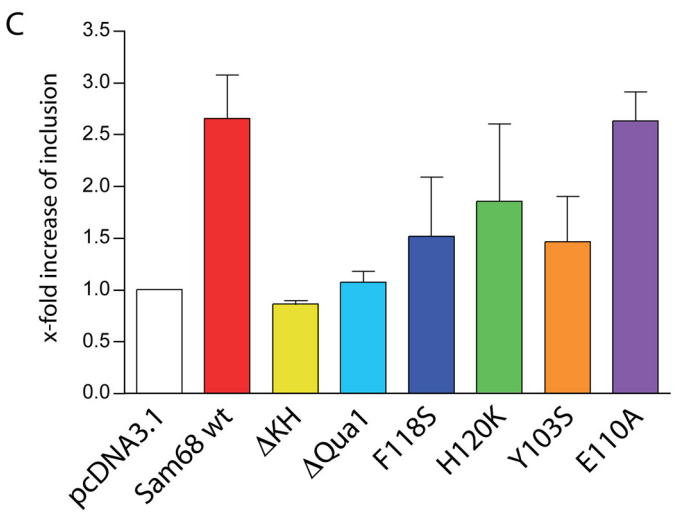


FIGURE 5. Mutational analysis of the Sam68 Qual domain reduces CD44 **exon v5 inclusion** in vivo. A, schematic presentation of the CD44 v5 minigene organization. Black boxes display the insulin exons (Ex); the gray box represents CD44 exon v5. PCR primer positions are indicated as arrows. Inclusion of CD44 v5 leads to a PCR product with a predicted size of 361 bp, whereas exclusion of exon v5 results in a 244-bp PCR product. B, RT-PCR analysis of minigene splicing patterns from cytoplasmic RNA of U138MG cells co-transfected with the CD44 v5 minigene construct pETv5 (13) and with plasmids for expression of wild type or mutant Sam68 proteins. Cells were co-transfected with the minigene construct and the empty vector plasmid (pcDNA3.1) as control. The expression levels of a housekeeping gene (RNA polymerase II) are shown for comparison. Values for exon inclusion (expressed as the percentage of variant exon-containing RT-PCR products relative to total RT-PCR products) are displayed. C, RT-PCR bands were quantified densitometrically using the ImageJ Software. Each Sam68 protein was assayed in three independent co-transfection experiments. The graph shows the x-fold increase of the percentage of exon inclusion for the RT-PCR products in U138MG cells, relative to the control. Columns represent the mean results of three independent experiments, and error bars represent the S.E.

that the Qua1 domain is the main determinant for the dimerization of Sam68. In any case, our results unequivocally show that the Qua1 domain is required for the functional activity in splicing regulation of Sam68 in vivo. Thus, dimerization of Sam68 is at least as important for splicing as the binding to the target RNA itself, which is mediated by the KH-Qua2 domain. As the surface of Qua1 is negatively charged (Fig. 3D), it is unlikely that the Qua1 domain contributes directly to RNA binding. Instead, Qua1 homodimerization may bring together



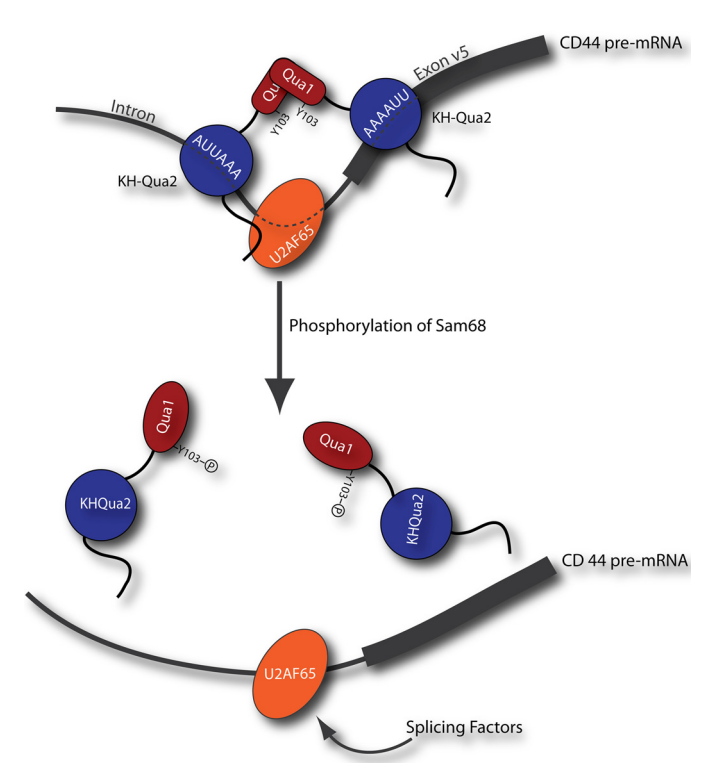


FIGURE 6. Model of the Sam68 interaction with CD44 pre-mRNA and U2AF65. Sam68 dimerization via the Qua1 domain may allow simultaneous binding to cognate RNA elements in the CD44 exon v5 and the preceding intron. Phosphorylation of Sam68 has been shown to reduce the RNA binding affinity and thus releases Sam68 from the pre-mRNA. This is required for recruiting constitutive splicing factors and spliceosome assembly. Phosphorylation of Tyr-103 might contribute to the release of Sam68 from the pre-mRNA by destabilizing the dimerization via Qua1.

two KH-Qua2 domains for recognition of bipartite RNA sequences (Fig. 6), a conserved feature within the STAR family.

With respect to alternative splicing of the CD44 v5 exon, Qua1 dimerization may serve two functions. Firstly, it could stabilize binding to two independent RNA binding sites, one within exon v5 and one in the preceding intron, thus promoting splice site definition by other factors. For instance, Sam68 stabilizes binding of U2AF65 to the CD44 pre-mRNA (Fig. 6), which has no canonical U2AF65 binding site downstream of the branch point RNA sequence (9). Secondly, Sam68 appears to promote rearrangement of the spliceosome by leaving the protein-RNA complex. It has been postulated that this is facilitated by a reduced RNA binding affinity linked to phosphorylation (9).

Phosphorylation of Tyr-103 might act as a possible switch in disassembling the Sam68 dimer and thus releasing the protein from the CD44 pre-mRNA (Fig. 6). The Y103S mutation in Sam68 only partially affects the structural integrity *in vitro* (Fig. 4B, supplemental Fig. 5), whereas our *in vivo* splicing assays indicate that Tyr-103 is critical for Sam68 function as it strongly reduces exon v5 inclusion on the CD44 mRNA. The loss of splicing activity is comparable with the F118S mutation, which completely destabilizes the dimeric fold. This cannot be explained exclusively by the modest effect of the Y103S mutation on dimerization of Qua1 *in vitro*. One possible explanation for this paradox might be the potential phosphorylation of Tyr-103 by a tyrosine kinase (50). Because Tyr-103 is located close to the

edge of the dimer interface, it is in principle accessible to phosphorylation by a kinase. Phosphorylation could sterically interfere with the dimerization. Additionally, the intermolecular hydrogen-bond network, which we have shown to be crucial for dimerization, could be disturbed by additional hydrogen-bond acceptors and donors provided by the phosphate group. Finally, the additional negative charge of the phosphate might lead to repulsion of the two monomers and thereby destabilize the dimer. Phosphorylation of Tyr-103 might thus play a role for the Sam68 splicing activity, beyond this residue being important for the stability of the Qua1 dimer. Future studies should focus on understanding the molecular mechanisms of the function of the Sam68 STAR domain and its modulation by phosphorylation.

Acknowledgments—We thank Harald König, Karlsruhe Institute of Technology (KIT), for providing Sam68 expression vectors and CD44 minigene constructs and Serge Storz for cloning of the initial Qua1 construct. We thank the Bavarian NMR Centre (BNMRZ) for NMR time.

REFERENCES

- 1. Taylor, S. J., and Shalloway, D. (1994) Nature 368, 867–871
- 2. Lukong, K. E., and Richard, S. (2003) Biochim. Biophys. Acta 1653, 73-86
- 3. Vernet, C., and Artzt, K. (1997) Trends Genet 13, 479 484
- Najib, S., Martín-Romero, C., González-Yanes, C., and Sánchez-Margalet, V. (2005) Cell Mol. Life Sci. 62, 36 – 43
- Pillay, I., Nakano, H., and Sharma, S. V. (1996) Cell Growth Differ. 7, 1487–1499
- Lin, Q., Taylor, S. J., and Shalloway, D. (1997) J. Biol. Chem. 272, 27274–27280
- Itoh, M., Haga, I., Li, Q. H., and Fujisawa, J. (2002) Nucleic Acids Res. 30, 5452–5464
- 8. Wang, L. L., Richard, S., and Shaw, A. S. (1995) J. Biol. Chem. 270, 2010-2013
- 9. Tisserant, A., and König, H. (2008) PLoS One 3, e1418
- 10. Guitard, E., Barlat, I., Maurier, F., Schweighoffer, F., and Tocque, B. (1998) *Biochem. Biophys. Res. Commun.* **245**, 562–566
- 11. Babic, I., Jakymiw, A., and Fujita, D. J. (2004) Oncogene 23, 3781-3789
- Busà, R., Paronetto, M. P., Farini, D., Pierantozzi, E., Botti, F., Angelini,
 D. F., Attisani, F., Vespasiani, G., and Sette, C. (2007) Oncogene 26, 4372–4382
- 13. Matter, N., Herrlich, P., and König, H. (2002) Nature 420, 691-695
- Paronetto, M. P., Achsel, T., Massiello, A., Chalfant, C. E., and Sette, C. (2007) J. Cell Biol. 176, 929–939
- Arch, R., Wirth, K., Hofmann, M., Ponta, H., Matzku, S., Herrlich, P., and Zöller, M. (1992) Science 257, 682–685
- 16. Cooper, D. L., and Dougherty, G. J. (1995) Nat. Med. 1, 635-637
- 17. Sherman, L., Sleeman, J., Dall, P., Hekele, A., Moll, J., Ponta, H., and Herrlich, P. (1996) *Curr. Top. Microbiol. Immunol.* 213, 249–269
- Sherman, L., Wainwright, D., Ponta, H., and Herrlich, P. (1998) *Genes Dev.* 12, 1058 – 1071
- Weg-Remers, S., Ponta, H., Herrlich, P., and König, H. (2001) EMBO J. 20, 4194 – 4203
- Berglund, J. A., Chua, K., Abovich, N., Reed, R., and Rosbash, M. (1997)
 Cell 89, 781–787
- 21. Burd, C. G., and Dreyfuss, G. (1994) Science 265, 615-621
- Liu, Z., Luyten, I., Bottomley, M. J., Messias, A. C., Houngninou-Molango, S., Sprangers, R., Zanier, K., Krämer, A., and Sattler, M. (2001) *Science* 294, 1098 – 1102
- 23. Maguire, M. L., Guler-Gane, G., Nietlispach, D., Raine, A. R., Zorn, A. M., Standart, N., and Broadhurst, R. W. (2005) *J. Mol. Biol.* **348**, 265–279
- 24. Zorn, A. M., and Krieg, P. A. (1997) Genes Dev. 11, 2176-2190
- 25. Chen, T., Damaj, B. B., Herrera, C., Lasko, P., and Richard, S. (1997) Mol.



- Cell. Biol. 17, 5707-5718 26. Di Fruscio, M., Chen, T., and Richard, S. (1999) Proc. Natl. Acad. Sci.
- *U.S.A.* **96,** 2710 2715 27. Wu, J., Zhou, L., Tonissen, K., Tee, R., and Artzt, K. (1999) J. Biol. Chem.
- 274, 29202-29210 28. Delaglio, F., Grzesiek, S., Vuister, G. W., Zhu, G., Pfeifer, J., and Bax, A.
- (1995) J. Biomol. NMR 6, 277–293 29. Goddard, T., and Kneller, D. (2007) SPARKY 3, University of California,
- San Francisco
- 30. Jung, Y. S., and Zweckstetter, M. (2004) J. Biomol. NMR 30, 11-23
- 31. Sattler, M., Schleucher, J., and Griesinger, C. (1999) Prog. Nucl. Magn. Reson. Spectrosc. 34, 93-158
- 32. Otting, G., and Wüthrich, K. (1990) Q. Rev. Biophys. 23, 39-96
- 33. Farrow, N. A., Muhandiram, R., Singer, A. U., Pascal, S. M., Kay, C. M., Gish, G., Shoelson, S. E., Pawson, T., Forman-Kay, J. D., and Kay, L. E. (1994) Biochemistry 33, 5984 - 6003
- 34. Yang, D., Venters, R. A., Mueller, G. A., Choy, W. Y., and Kay, L. E. (1999) J. Biomol. NMR 14, 333-343
- 35. Rückert, M., and Otting, G. (2000) J. Am. Chem. Soc. 122, 7793-7797
- 36. Madl, T., Bermel, W., and Zangger, K. (2009) Angew. Chem. Int. Ed Engl. **48**, 8259 – 8262
- 37. Güntert, P. (2009) Eur. Biophys. J. 38, 129-143
- 38. Nilges, M. (1993) Proteins 17, 297-309
- 39. Shen, Y., Delaglio, F., Cornilescu, G., and Bax, A. (2009) J. Biomol. NMR 44, 213-223
- 40. Linge, J. P., Williams, M. A., Spronk, C. A., Bonvin, A. M., and Nilges, M. (2003) Proteins 50, 496-506

- 41. Rieping, W., Habeck, M., Bardiaux, B., Bernard, A., Malliavin, T. E., and Nilges, M. (2007) Bioinformatics 23, 381-382
- 42. Lipsitz, R. S., and Tjandra, N. (2004) Annu. Rev. Biophys. Biomol. Struct. 33, 387-413
- 43. Laskowski, R. A., Rullmannn, J. A., MacArthur, M. W., Kaptein, R., and Thornton, J. M. (1996) J. Biomol. NMR 8, 477-486
- 44. Hooft, R. W., Vriend, G., Sander, C., and Abola, E. E. (1996) Nature 381, 272
- 45. DeLano, W. L. (2002) The PyMOL Molecular Graphics System, DeLano Scientific LLC, San Carlos, CA
- 46. Hadian, K., Vincendeau, M., Mäusbacher, N., Nagel, D., Hauck, S. M., Ueffing, M., Loyter, A., Werner, T., Wolff, H., and Brack-Werner, R. (2009) J. Biol. Chem. 284, 33384-33391
- 47. Krissinel, E., and Henrick, K. (2004) Acta Crystallogr. D. Biol. Crystallogr. **60,** 2256 – 2268
- 48. Li, J., Liu, Y., Park, I. W., and He, J. J. (2002) J. Virol. 76, 4526-4535
- 49. Beuck, C., Szymczyna, B. R., Kerkow, D. E., Carmel, A. B., Columbus, L., Stanfield, R. L., and Williamson, J. R. (2010) Structure 18, 377-389
- Richard, S., Yu, D., Blumer, K. J., Hausladen, D., Olszowy, M. W., Connelly, P. A., and Shaw, A. S. (1995) Mol. Cell. Biol. 15, 186-197
- 51. Thompson, J. D., Gibson, T. J., and Higgins, D. G. (2002) in Current Protocols in Bioinformatics (Baxevanis, A. D., ed) John Wiley & Sons, Inc.,
- 52. Gouet, P., Courcelle, E., Stuart, D. I., and Métoz, F. (1999) Bioinformatics **15,** 305–308
- 53. Baker, N. A., Sept, D., Joseph, S., Holst, M. J., and McCammon, J. A. (2001) Proc. Natl. Acad. Sci. U.S.A. 98, 10037-10041

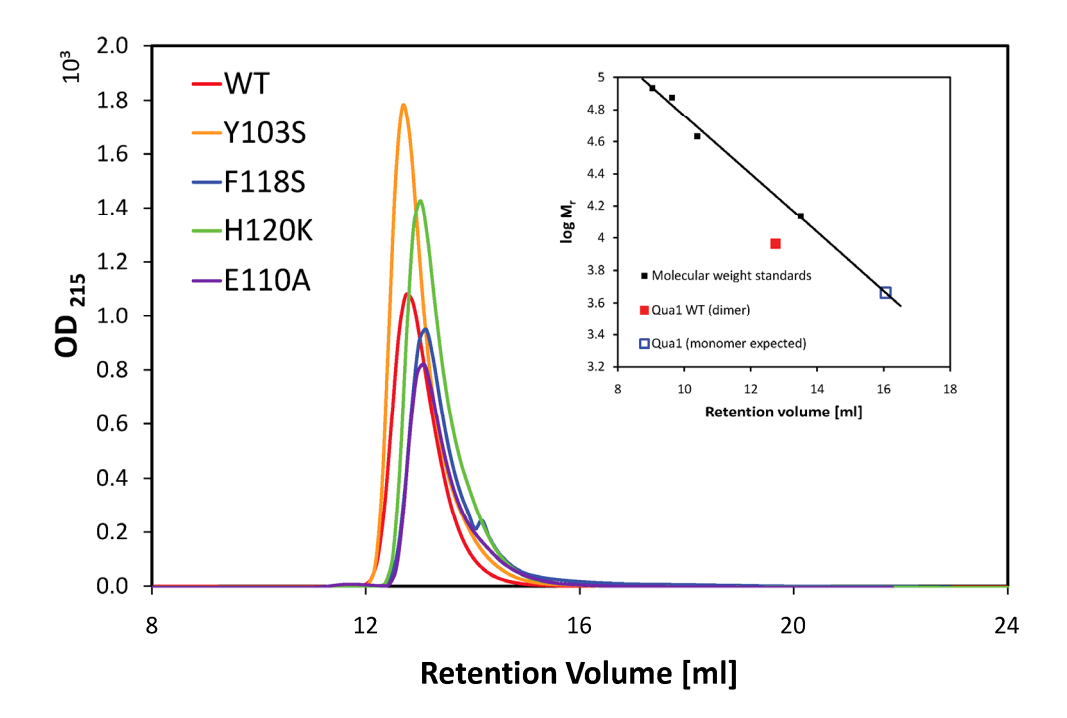


Supplemental Figures

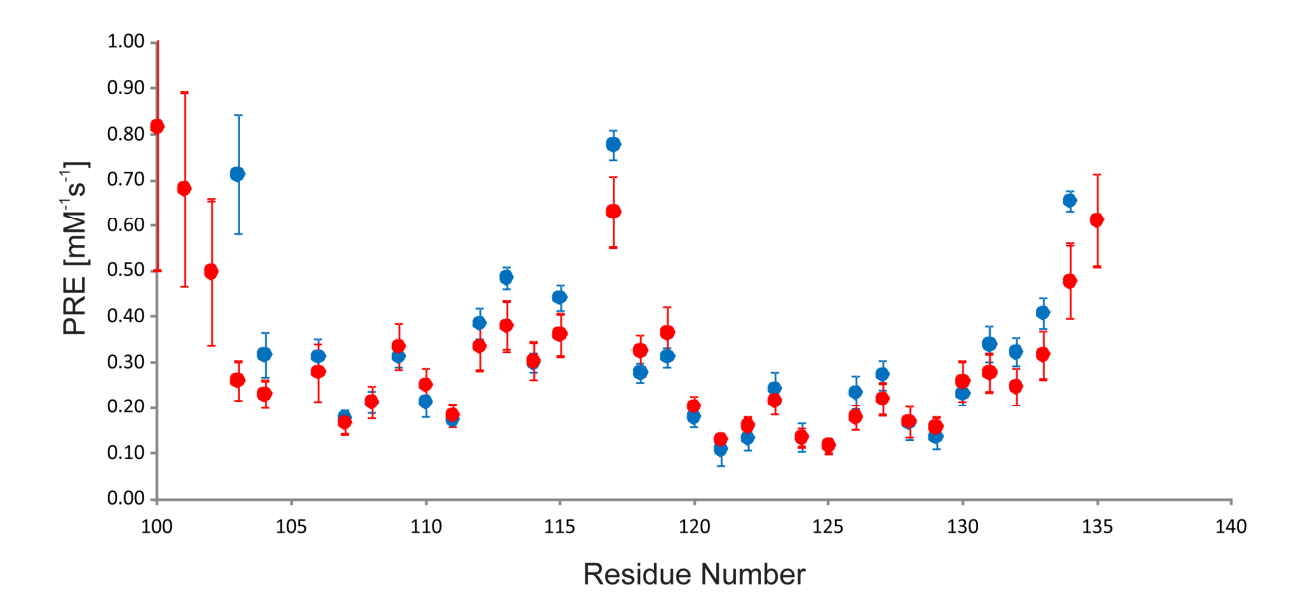
Structural basis for homodimerization of the Src-associated during mitosis, 68 kDa protein (Sam68) Qual domain

N. Helge Meyer ^{1,2}, Konstantinos Tripsianes ^{1,2}, Michelle Vincendeau³, Tobias Madl^{1,2}, Fatiha Kateb^{1,2}, Ruth Brack-Werner³, Michael Sattler^{1,2}

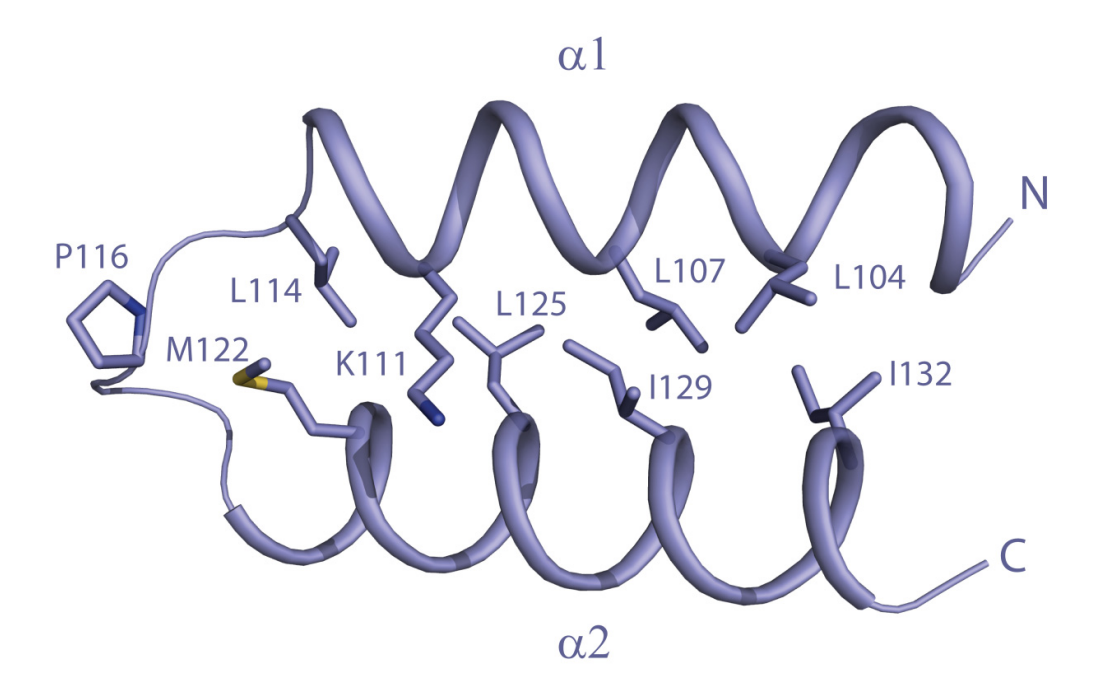
Supplementary Figure 1



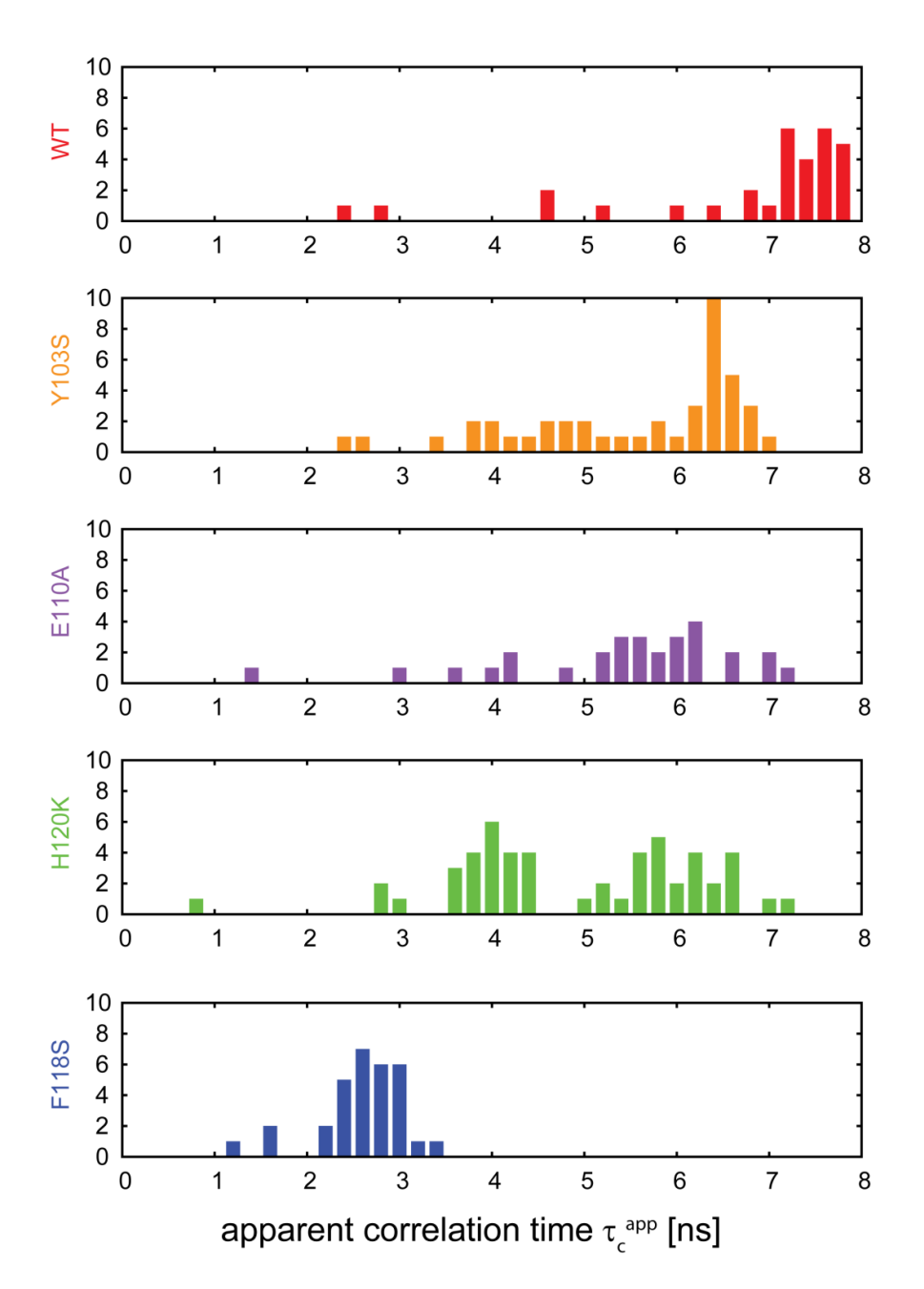
Supplementary Figure 1: Size exclusion chromatography of Sam68 wildtype as well as Y103S, F118S, H120K and E110A variants. Proteins were loaded onto a Superdex 75 10/300 gel filtration column (GE Healthcare). Molecular weight was calibrated with standard proteins: Ribonuclease A (13.7 kDa), Ovalbumine (43.0 kDa monomer, 86 kDa dimer) and Conalbumine (75 kDa) (GE Healthcare). The retention volumes of wild type and the Y103S mutant proteins correspond well to that expected for a dimer. The F118S, H120K and E110A variants have a slightly increased retention volume compared to the wild type, which, however, does not match the retention volume expected for a globular monomeric form of the protein. This may reflect that the mutants are destabilized and/or unfolded resulting in an increased hydrodynamic radius.



Supplementary Figure 2: Paramagnetic relaxation enhancements (PREs) for the backbone amide protons of Qua1. Measured PREs (blue) and PREs back-calculated for the ensemble of NMR structures (red). For some surface protons – particularly protons located in loops and the flexible termini– the measured PRE is higher than calculated. This is due to chemical exchange between these protons and water protons. Water is coordinated to gadolinium in Gd(DTPA-BMA) and thus experiences large relaxation enhancements. As this water ligand exchanges with free water and then to amide protons the large relaxation enhancement is partly transferred.

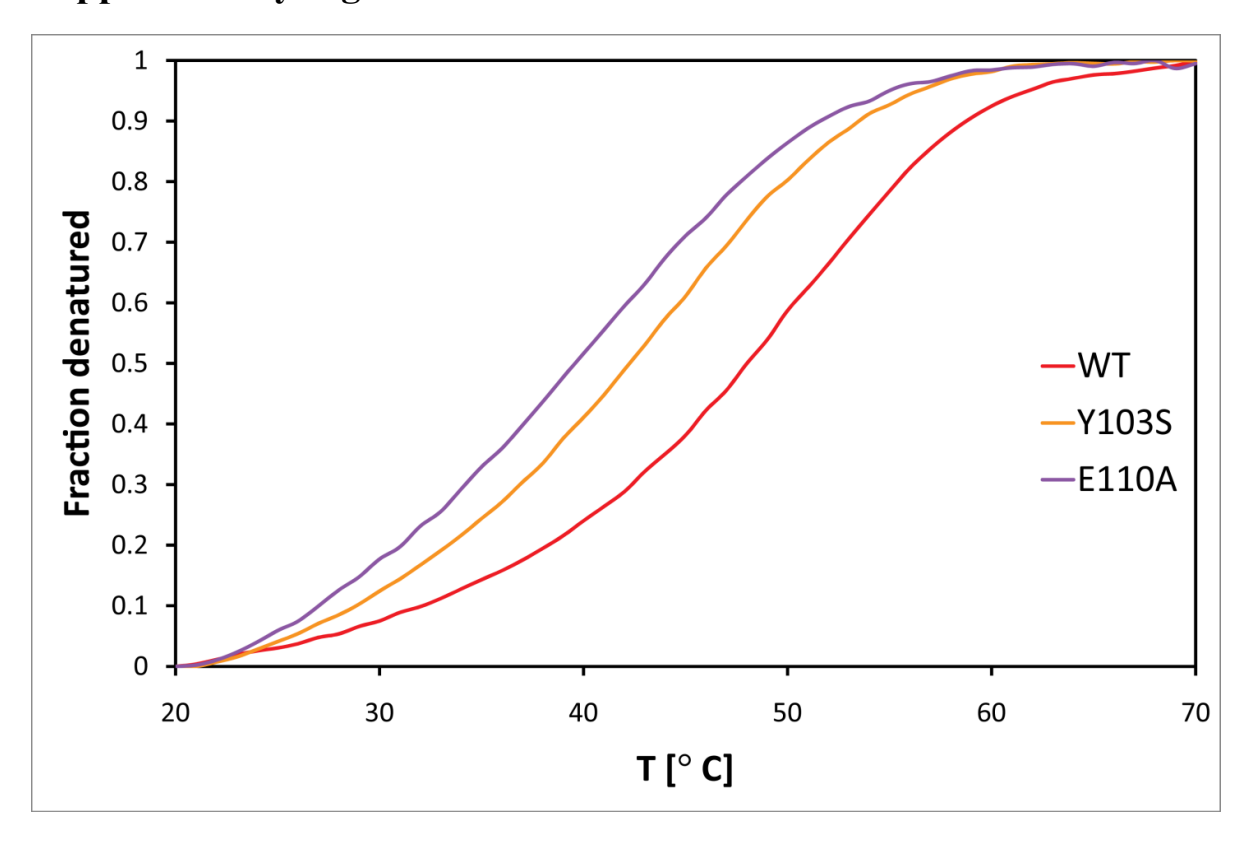


Supplementary Figure 3: Ribbon representation of a Qua1 monomer. Side chains of residues, which stabilize the helical hairpin, are shown as sticks.



Supplementary Figure 4: Histograms of apparent correlation times (τ_c^{app}) derived from ¹⁵N relaxation data for Sam68 Qua1 (residues 95-135). Apparent local correlation times were calculated from the ¹⁵N R₂/R₁ relaxation rate ratios. The average τ_c^{app} for the wild type Qua1 is consistent with a homodimer, whereas the reduced values for the mutants indicate that dimerization is disturbed. F118S, which is unfolded and monomeric, has the lowest average correlation time. All other mutants show correlation times in between those of F118S and wild type.

Note, that the very small correlation times for wild type Qual arise from flexible regions of the protein.



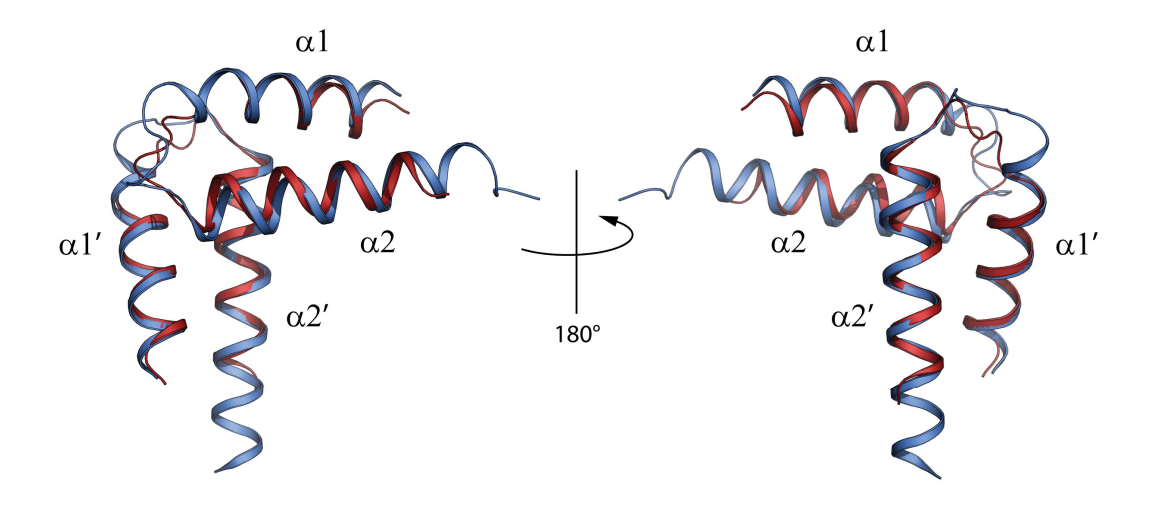
Supplementary Figure 5: Thermal denaturation of Sam68 Qual WT and E110A and Y103S variants. Thermal denaturation was monitored by CD spectroscopy. The fraction of denatured protein was determined by measuring molar ellipticity θ at 222 nm at steps of 1° C (heating rate 2° C min⁻¹).

Downloaded from www.jbc.org at Helmholtz Zentrum Muenchen - Zentralbibliothek, on November 3, 2010

Supplementary Figure 6



Supplementary Figure 6: Sam68 expression in U138MG and HeLa cells. Western Blot analysis of U138MG and HeLa cell lysates show significant more endogenous Sam68 expression in HeLa cells compared to the astrocytic U138MG cells. GAPDH western blot served as a loading control.



Supplementary Figure 7: Superposition of the Sam68 Qua1 (red) and Gld-1 Qua1 (blue) structures. Backbone atoms of residues 100-114 ($\alpha1$), 115-116 (linker) and 117-134 ($\alpha2$) of Sam68 Qua1 are aligned with the respective residues 146-160 ($\alpha1$), 163-164 (linker) and 166-183 ($\alpha2$) of Gld-1 Qua1. The two structures superimpose with a backbone coordinate RMSD of 1.1 Å. The sequence identity of the Qua1 domains of the two proteins is 23%. Note, that in the linker region only P116 is conserved.